ISSN 1674-1056
http://cpb.iphy.ac.cn
http://iopscience.iop.org/cpb
中国物理 B
Chinese Physics
中国物理 Chinese Physics B

Monolithic all-fiber mid-infrared supercontinuum source based on a step-index two-mode As_2S_3 fiber

Jinmei Yao(姚金妹), Bin Zhang(张斌), Jing Hou(侯静)

Citation: Chin. Phys. B . 2019, 28(6): 064205. **doi:** 10.1088/1674-1056/28/6/064205
Journal homepage: http://cpb.iphy.ac.cn; http://iopscience.iop.org/cpb

What follows is a list of articles you may be interested in

Supercontinuum generation of highly nonlinear fibers pumped by 1.57-μm laser soliton

Song-Tao Fan(樊松涛), Yan-Yan Zhang(张颜艳), Lu-Lu Yan(闫露露), Wen-Ge Guo(郭文阁), Shou-Gang Zhang(张首刚), Hai-Feng Jiang(姜海峰)

Chin. Phys. B . 2019, 28(6): 064204. **doi:** 10.1088/1674-1056/28/6/064204

Mid-infrared supercontinuum generation and its application on all-optical quantization with different input pulses

Yan Li(李妍), Xinzhu Sang(桑新柱)

Chin. Phys. B . 2019, 28(5): 054206. **doi:** 10.1088/1674-1056/28/5/054206

Supercontinuum manipulation based on the influence of chirp on soliton spectral tunneling

Saili Zhao(赵赛丽), Huan Yang(杨华), Yilin Zhao(赵奕霖), Yuzhe Xiao(肖宇哲)

Chin. Phys. B . 2018, 27(11): 114219. **doi:** 10.1088/1674-1056/27/11/114219

Intense supercontinuum generation in the near-ultraviolet range from a 400-nm femtosecond laser filament array in fused silica

Dongwei Li(李东伟), Lanzhi Zhang(张兰芝), Saba Zafar, He Song(宋鹤), Zuoqiang Hao(郝作强), Tingting Xi(奚婷婷), Xun Gao(高勋), Jingquan Lin(林景全)

Chin. Phys. B . 2017, 26(7): 074213. **doi:** 10.1088/1674-1056/26/7/074213

Numerical investigation on broadband mid-infrared supercontinuum generation in chalcogenide suspended-core fibers

Kundong Mo(莫坤东), Bo Zhai(翟波), Jianfeng Li(李剑峰), E Coscelli, F Poli, A Cucinotta, S Selleri, Chen Wei(韦晨), Yong Liu(刘永)

Chin. Phys. B . 2017, 26(5): 054216. **doi:** 10.1088/1674-1056/26/5/054216

Monolithic all-fiber mid-infrared supercontinuum source based on a step-index two-mode As_2S_3 fiber*

Jinmei Yao(姚金妹)[1], Bin Zhang(张斌)[1,2,3,†], and Jing Hou(侯静)[1,2,3]

[1] College of Advanced Interdisciplinary Studies, National University of Defense Technology, Changsha 410073, China
[2] State Key Laboratory of Pulsed Power Laser Technology, Changsha 410073, China
[3] Hunan Provincial Key Laboratory of High Energy Laser Technology, Changsha 410073, China

(Received 14 December 2018; revised manuscript received 11 February 2019; published online 8 May 2019)

We demonstrate efficient supercontinuum generation extending into mid-infrared spectral range by pumping a two-mode As_2S_3 fiber in the normal dispersion regime. The As_2S_3 fiber is fusion spliced to the pigtail of a near-infrared supercontinuum pump source with ultra-low splicing loss of 0.125 dB, which enables a monolithic all-fiber mid-infrared supercontinuum source. By two-mode excitation and mixed-mode cascaded stimulated Raman scattering, a supercontinuum spanning from 1.8 μm to 4.2 μm is obtained. Over 70% of the supercontinuum power is converted to wavelengths beyond 2.4 μm. This is the first experimental report with respect to the multimode mid-infrared supercontinuum generation in a step-index two-mode chalcogenide fiber.

Keywords: supercontinuum generation, infrared lasers, fiber lasers, nonlinear.

PACS: 42.55.Wd, 42.81.–i, 42.65.Ky **DOI:** 10.1088/1674-1056/28/6/064205

1. Introduction

Mid-infrared (MIR) supercontinuum (SC) sources have attracted a significant scientific interest in the past decade due to their wide range of potential applications in fields such as optical coherence tomography,[1] chemical sensing,[2] biomedical imaging and early cancer diagnostics.[3–5] Generally, the SC spectra generated in silica fibers struggle to exceed 2.4 μm due to the limited optical transparency of silica glass. To create SC generation tailing to a longer wavelength region, GeO_2-doped fibers with extended transmission window up to $\sim$ 3.6 μm are used.[6] To further extend the spectra of SC laser sources beyond 4 μm, soft-glass fibers, such as fluoride fibers,[7,8] tellurite fibers,[9] and chalcogenide fibers, are much more suitable. Specifically, chalcogenide glass fibers facilitating broadband transmittance window and high nonlinear refractive index n_2 in the infrared region,[10,11] become the most promising medium for MIR SC generation towards far-infrared spectral range. However, typical chalcogenide fibers have large material zero dispersion wavelengths (ZDWs). The material ZDWs of As_2S_3 glass and As_2Se_3 glass are located at $\sim$ 4.8 μm and 8 μm,[10] respectively. These ZDWs are far away from the commercial laser sources. Therefore, in order to obtain MIR SC laser sources effectively, chalcogenide fibers with high numerical apertures (NAs) are needed to lower the ZDWs meanwhile confine MIR light in the core of fibers.[12] But the risk is that higher-order modes (HOMs) tend to be excited in the near-infrared and shortwave-infrared spectral range. Such excitation of HOM is often neglected in previous chalcogenide fiber-based SC studies. Compared with the fundamental mode, HOMs exhibit different dispersion curves and nonlinear indices, which are the most important factors for SC generation. In addition, intermodal nonlinear effects taken place through cross-phase modulation,[13] four-wave mixing[14,15] and stimulated Raman scattering,[16] offer an additional possibility for spectral broadening through new degrees of freedom. Hence, it is necessary to investigate HOM SC generation in few-mode chalcogenide fibers. Visible and near-infrared SC generation have been carried out in micro-structured multimode silica fibers[17–19] and graded-index multimode silica fibers,[20–22] while an MIR SC demonstration has been reported in a ZBLAN fiber with anomalous dispersion.[23] Numerical simulations related to multimode SC generation in chalcogenide fibers have been demonstrated,[12,24] yet there are still no explicit experimental validations.

Fiber-based SC laser sources benefit from their compact configuration that are needed for robust commercial applications. Compared with lens coupling and butt-coupling, fusion splicing with permanent and robust connection is the best coupling method for fiber-based SC laser. However, it is difficult to achieve a real-all-fiber structured MIR SC laser source based on chalcogenide glass fibers. The glass transition temperature is 1215 °C for silica glass, while it is 130 °C$\sim$ 300 °C for chalcogenide glasses.[5] The significant difference in the two fibers' glass transition temperatures brings a great challenge for fusion splicing them together. The asymmetric heating configuration has been proved as an efficient method for

*Project supported by the National Natural Science Foundation of China (Grant Nos. 61435009, 61235008, and 61405254).
†Corresponding author. E-mail: nudtzhb@163.com
© 2019 Chinese Physical Society and IOP Publishing Ltd

splicing fibers with discrepant transition temperatures.[25–27] In this method, the silica fiber is fusion spliced to the chalcogenide fiber with 0.5 dB of splice loss.[26]

In this paper, we demonstrate MIR SC sources spanning from 1.8 μm to 4.2 μm using a step-index two-mode As_2S_3 fiber. The asymmetric heating method is used for fusion splicing between the As_2S_3 fiber and the pigtail of near-infrared SC pump source with an ultra-low insertion loss of 0.125 dB, which enables a monolithic all-fiber structured SC laser. The measured beam profile reveals that LP_{11} mode is excited within a wide spectral range of 1.8 μm–3.5 μm. The mixed-mode cascaded stimulated Raman scattering with respect to the fundamental mode and the off-center-alignment-induced LP_{11} mode, mainly contribute to the spectral broadening.

2. Experimental setup

The experimental setup of the pump source is similar to the structure described in Ref. [25]. The pump source is a nanosecond shortwave-infrared SC laser with a repetition rate of 100 kHz and a spectral range of 1.9 μm–2.5 μm (see Fig. 1). Note that the majority power of the pump light is located within the spectral range of 2.1 μm–2.2 μm. The pigtail fiber of the pump source is an ultra-high numerical aperture (UHNA) fiber with a core/cladding diameter of 2.2 μm/125 μm and an NA of 0.35. The V-number of UHNA fiber is 1.1 at around 2.19 μm, which ensures that the shortwave infrared region holds the single-mode property. A 3-m-long sulfide-based chalcogenide fiber is chosen as the nonlinear fiber due to its lower ZDW than that of selenide-based chalcogenide fibers. The core/cladding diameter of the step-index As_2S_3 fiber is 9 μm/170 μm with an NA of 0.3. Since the V-number of the As_2S_3 fiber is 3.87 at around 2.19 μm, the SC generation behaves at few-mode scheme, where LP_{11} mode with cut-off wavelength of 3.5 μm is the dominant HOM in MIR spectral range. The group-velocity dispersion of the fundamental mode and the LP_{11} mode can be found in Ref. [28]. The estimated ZDW for the fundamental mode reaches 6.7 μm, while the LP_{11} mode facilitates normal dispersion over the whole MIR spectral range. By using the commercial software (COMSOL Multiphysics), the mode field diameters of the UHNA fiber and the As_2S_3 fiber, corresponding to the fundamental mode at 2.19 μm, are estimated to be 7.77 μm and 7.99 μm, respectively. The mode profile mismatch between the two fibers is less than 0.01%, indicating a great potential of low-loss fusion splicing of UHNA fiber to the As_2S_3 fiber for integrated MIR SC laser source.

During the fusion splicing, an electrode-based fiber fusion splicer is used to achieve the accurate control of the temperature field, while a continuous-wave fiber laser operating at 1960 nm is adopted to monitor the coupling efficiency. The end facet of the As_2S_3 fiber is angle-cleaved to suppress the unwanted optical feedback from the Fresnel reflection. Figure 2(a) shows the transmission of the splicing point under 1960-nm continuous-wave laser, in which the inset shows the optical microscope image of the fusion splicing joint between the UHNA fiber and the As_2S_3 fiber. Figure 2(a) shows that the coupling efficiency is enhanced along with the increase of continuous-wave power due to the thermal expansion of the core of As_2S_3 fiber. An approximate transmission of 63% is measured at the end of the As_2S_3 fiber. Since the Fresnel reflection loss between UHNA fiber ($n_0 = 1.438$ at 2 μm) and As_2S_3 fiber ($n_0 = 2.426$ at 2 μm) is about 0.3 dB. The Fresnel reflection loss on the output end facet of As_2S_3 fiber is about 0.825 dB. Thus, the fusion splicing loss is estimated to be ~ 0.125 dB, by taking the linear propagation loss at 2 μm (0.25 dB/m) into account. Figures 2(b) and 2(c) show the end facet of As_2S_3 fiber and UHNA fiber after pulling the joint apart, of which both end facets are well preserved during asymmetric heating and pushing processing.

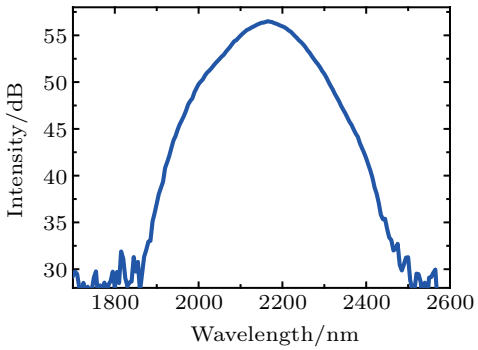


Fig. 1. Shortwave-infrared SC pump spectrum.

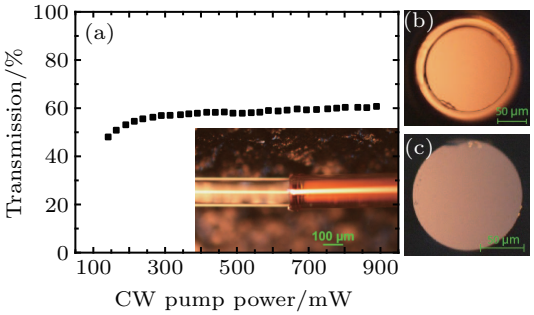


Fig. 2. (a) Transmission of the splicing point under continues-wave laser at 1960 nm. Inset: optical microscope images of the fusion splicing joint. The end facet of (b) As_2S_3 fiber and (c) UHNA fiber after pulling the joint apart.

3. Results and discussion

Figure 3(a) shows the spectral evolution in the As_2S_3 fiber as a function of average pump power, where the energy distribution asymmetrically shifts to the MIR region with the increase of pump power. When the average pump power reaches around 200 mW, an SC extending to 4.2 μm is obtained with an obvious dip at around 3.5 μm. Figure 3(b) shows the power

evolution of the MIR SC laser source, as well as the filtered SC power of wavelengths exceeding 2.4 μm. The maximal output power reaches 133 mW, meanwhile more than 70% of the output power is converted to the MIR region beyond 2.4 μm.

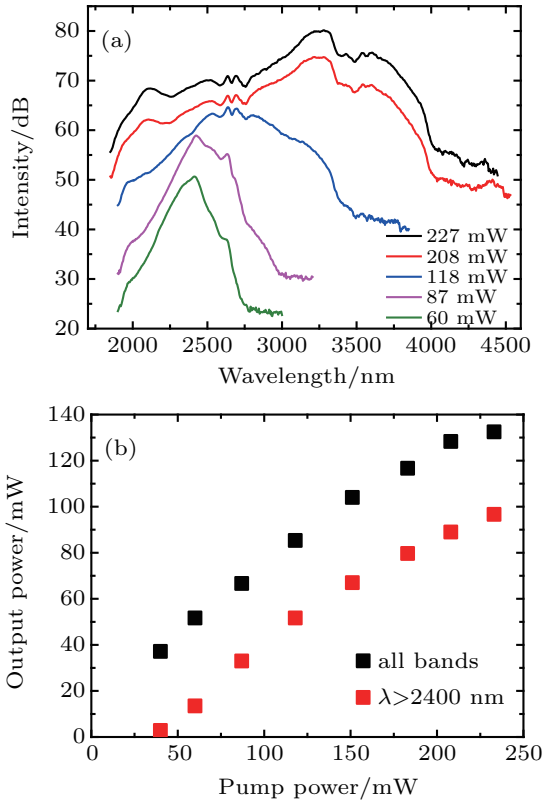


Fig. 3. (a) Spectral evolution of the SC as a function of average pump power (the corresponding launched pump powers are shown in the legend) and (b) output power versus average pump power in the 3-m-long As_2S_3 fiber with a core diameter of 9 μm.

The evolution of the beam profile of the SC source is characterized with a pyro-electric array camera (see Figs. 4(a)–4(c)), which shows that the excitation of LP_{11} mode is dominant in the primary stage (see Figs. 4(a) and 4(b)). Along with the spectrum broadening beyond 3.5 μm, the dominant state of LP_{11} mode is weak, as shown in Fig. 4(c). Since the V-number of the UHNA fiber is 1.1 at around 2.19 μm, it is single mode operation in the UHNA fiber. Thus, the mode conversion is achieved in the few-mode As_2S_3 fiber.

According to the spectral characters observed in Fig. 3(a) and the evolution of beam profile in Fig. 4, a possible explanation is given as follows. It is known that lateral misalignment and angular misalignment are easy to excite HOMs in a multimode fiber.[29] During the asymmetric heating process of pushing the UHNA fiber and the As_2S_3 fiber together, a precise coupling condition is hard to be guaranteed. Thus, it is possible to excite amount of LP_{11} mode in the input segment of the few-mode As_2S_3 fiber. After that, the energy of the mixed modes (LP_{01} and LP_{11}) is progressively shifted toward MIR region through propagation in the 3-m-long As_2S_3 fiber. According to 11-THz Stokes frequency shift of As_2S_3 fibers,[30] the first five Stokes-shifted orders corresponding to a pump wavelength of $\sim$ 2.2 μm are 2.4, 2.6, 2.9, 3.2, 3.7 μm, respectively. Although the Stokes peaks are inconspicuous in the generated spectra due to the broadband spectrum of pump light, the peaks located at 2.4, 2.6, 3.2, 3.7 μm can be figured out in Fig. 3(a) as well. Thus, stimulated Raman scattering is regarded as the dominant mechanism responsible for spectral broadening. With the output spectrum broadening beyond 3.5 μm, a well confinement of LP_{11} mode cannot be guaranteed in the core of As_2S_3 fiber, as shown in Fig. 4(c). Thus, there is a dip at around 3.5 μm in the spectra of Fig. 3(a) and a slight nonlinear dependence of the output power in Fig. 3(b). After completing the MIR SC experiment, the output end facet of the As_2S_3 fiber is checked under a microscope. There is no flaw or dust left on the output end facet of the As_2S_3 fiber, which verified that the beam profiles are correct.

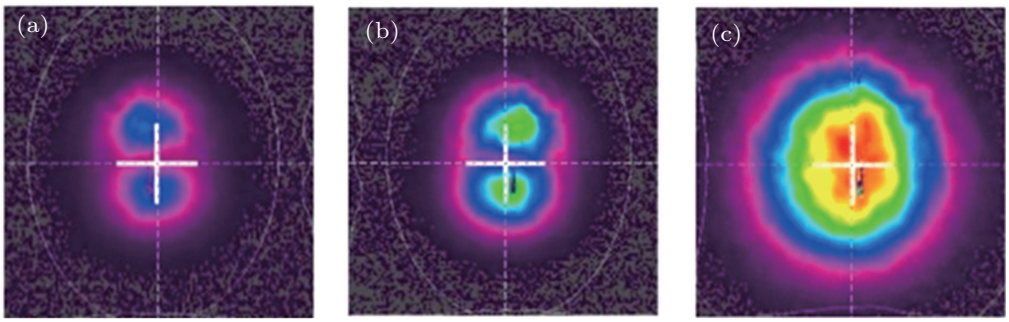


Fig. 4. Beam profiles of the SC source with the long wavelength region reach (a) 3 μm, (b) 3.5 μm, and (c) 4.2 μm.

A further spectral broadening through pump power scaling up is prohibited in the system. By further increasing the pump power, the output spectrum shrinks unexpectedly to 2 μm–2.5 μm and an obvious temperature rise is observed in the As_2S_3 fiber close to the splicing point with the use of a thermal camera. To make out the breakdown mechanism, the broken fusion-splicing joint is investigated under the optical microscope. The results are shown in Figs. 5(a)–5(d). This shows that although the splicing point cannot work properly, the fibers are still parallel alignment without separation and displacement (see Fig. 5(a)). While rotating the joint, a $\sim$ 90-μm-long short line is discovered in the center of the UHNA fiber, as shown in Figs. 5(b)–5(d).

The cross sections of the As_2S_3 fiber and UHNA fiber are observed under microscope after pulling the splicing joint apart. The end facets are shown in Figs. 6(a) and 6(b), which leave us some evidences of the breakdown mechanism. Figure 6(a) reveals that there is a distinct cavity like a 'crater' on the surface of the As_2S_3 fiber, which is approximately the same dimension as the core diameter (9 μm) of the As_2S_3 fiber. A mount of yellow gushing trace is observed on the end facet of UHNA fiber, as shown in Fig. 6(b), indicating a rapid vaporization of As_2S_3 glass has taken place.

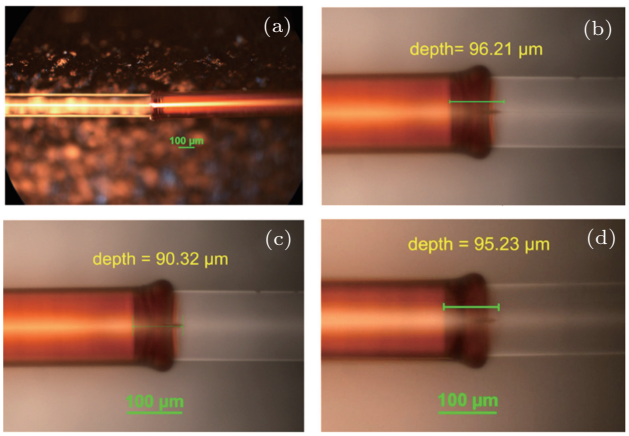


Fig. 5. (a) Optical microscope images of the fusion-splicing joint after pumped by nanosecond pulses. Panels (b)–(d) are the detailed images of the fusion splicing joint while rotating the splicing joint.

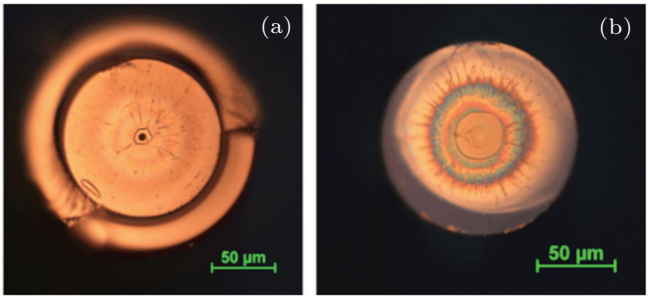


Fig. 6. The cross sections of (a) the As_2S_3 fiber and (b) the UHNA fiber after studies with nanosecond pulses.

Since the splicing joint works well under the continuous wave of about 900 mW but it breaks down pumped at 227 mW of the pulsed laser, a possible explanation is that the breakdown mechanism is related with the spectral broadening in the As_2S_3 fiber. The refractive index n_0 of As_2S_3 glass is around 2.42,[10] which leads to over 17% MIR light reflected on the output end facet of As_2S_3 fiber. Since the core NA of As_2S_3 fiber is 0.3, it is easy for the reflected MIR light back into the core and accumulates in the splicing joint. Hindered by the infrared absorption of UHNA glasses, energy of the reflected light is accumulated in the core of the splicing point. When the temperature rises to the transition temperature of As_2S_3 glass ($\sim$ 185 °C[31]), the core of the As_2S_3 fiber tends to be unstable and then a rapid vaporization takes place. Consequently, an obvious temperature rise is observed in the As_2S_3 fiber close to the splicing point and output spectrum shrunk to the spectrum of pump light. Thus, further damage mechanism such as fiber fuse[32] and effective methods to increase transmission at end facet of chalcogenide fiber such as antireflective surface structures[33] and anti-reflection coating[34] need to be explored to improve the steadiness of the all-fiber MIR SC source.

4. Conclusion

In conclusion, a 1.8-μm to 4.2-μm MIR SC is obtained in a two-mode As_2S_3 fiber. The measured beam profiles demonstrate that LP_{11} mode is excited within the wide spectral range between 1.8 μm to 3.5 μm. The dominant physical mechanism for spectral broadening in the two-mode As_2S_3 fiber is mixed-mode cascaded stimulated Raman scattering. Mode decomposition is needed in the future to make out the proportion of LP_{11} mode of the MIR SC source. In addition, an effective method to increase transmission at end facet of chalcogenide fiber is expected to improve the steadiness of the all-fiber MIR SC source.

Acknowledgment

We thank Dr. Tong Liu and Dr. Kai Guo for helpful discussions.

References

[1] Sergeeva E, Chang E W, Mattsson L, Kirillin M, Su R and Yun S H 2014 *Opt. Express* **22** 15804
[2] Kaminski C F, Watt R S, Elder A D, Frank J H and Hult J 2008 *Appl. Phys. B* **92** 367
[3] Seddon A B, Benson T M, Sujecki S, *et al.* 2016 *Proc. SPIE* **9703**
[4] Seddon A B 2013 *Phys. Status Solidi* **250** 1020
[5] Sanghera J S and Aggarwal I D 1999 *J. Non- Cryst. Solids* **256–257** 6
[6] Swiderski J 2014 *Prog. Quantum Electron.* **38** 189
[7] Yang Wei-Qiang Z B, Hou J, Yin Ke, Liu Z J 2014 *Chin. Phys. B* **23** 054208
[8] Yin K, Zhang B, Yang L and Hou J 2017 *Opt. Lett.* **42** 2334
[9] Kedenburg S, Strutynski C, Kibler B, Froidevaux P, Désévédavy F, Gadret G, Jules J C, Steinle T, Mörz F, Steinmann A, Giessen H and Smektala F 2017 *J. Opt. Soc. Am. B* **34** 601
[10] Ebendorff-Heidepriem H 2014 *OptoElectronics and Communication Conference and Australian Conference on Optical Fibre Technology*, 6 July, 2014, Melbourne, Australia, pp. 627–629
[11] Xiao-Yu Zhang F F C, Zhang X H and Wei J 2018 *Chin. Phys. B* **27** 084208
[12] Kubat I and Bang O 2016 *Opt. Express* **24** 2513
[13] Millot G, Pitois S, Dinda P T and Haelterman M 1997 *Opt. Lett.* **22** 1686
[14] Lesvigne C, Couderc V, Tonello A, Leproux P, Barthélémy A, Lacroix S, Druon F, Blandin P, Hanna M and Georges P 2007 *Opt. Lett.* **32** 2173
[15] Liu T, Chen S, Zhang B, Qi X, Liu W and Hou J 2014 *Appl. Phys. Express* **7** 062502
[16] Chiang K S 1992 *Opt. Lett.* **17** 352
[17] Vidne Y and Rosenbluh M 2005 *Opt. Express* **13** 9721
[18] Dudley J M, Provino L, Grossard N, Maillotte H, Windeler R S, Eggleton B J and Coen S 2002 *J. Opt. Soc. Am. B* **19** 765
[19] Shavrin I, Novotny S and Ludvigsen H 2013 *Opt. Express* **21** 32141

[20] Wright L G, Christodoulides D N and Wise F W 2015 *Nat. Photon.* **9** 306
[21] Krupa K, Louot C, Couderc V, Fabert M, Guenard R, Shalaby B M, Tonello A, Pagnoux D, Leproux P and Bendahmane A 2016 *Opt. Lett.* **41** 5785
[22] Lopez-Galmiche G, Sanjabi E Z, Eftekhar M A, Antonio L J, Wright L G, Wise F, Christodoulides D and Amezcua C R 2016 *Opt. Lett.* **41** 2553
[23] Ramsay J, Dupont S, Johansen M, Rishøj L, Rottwitt K, Moselund P M and Keiding S R 2013 *Opt. Express* **21** 10764
[24] Chen L, Gao W, Chen L, Wang P, Ni C, Chen X, Zhou Y, Zhang W, Hu J, Liao M, Suzuki T and Ohishi Y 2018 *Appl. Opt.* **57** 382
[25] Yin K, Zhang B, Yao J, Yang L, Chen S and Hou J 2016 *Opt. Lett.* **41** 946
[26] Rajesh T, Gattass R R, Vinh N, Geoff C, Dan G, Woohong K, L Brandon S and Sanghera J S 2015 *Opt. Lett.* **40** 5074
[27] Zheng Z J , Ouyang D Q , Zhao J Q , Ruan S C , Yu J, Guo C Y and Wang J Z 2015 *Chin. Phys. Lett.* **32** 114206
[28] Yao J, Zhang B, Yin K, Yang L, Hou J and Lu Q 2016 *Opt. Express* **24** 14717
[29] Grosjean T, Courjon D and Spajer M 2002 *Opt. Commun.* **203** 1
[30] Xiong C, Magi E, Luan F, Tuniz A, Dekker S, Sanghera J S, Shaw L B, Aggarwal I D and Eggleton B J 2009 *Appl. Opt.* **48** 5467
[31] Shiryaev V S and Churbanov M F 2013 *J. Non·Cryst. Solids* **377** 225
[32] Xing S, Kharitonov S, Hu J and Brès C S 2018 *Opt. Lett.* **43** 1443
[33] Lotz M R, Petersen C R, Markos C, Bang O, Jakobsen M H and Taboryski R 2018 *Optica* **5** 557
[34] Sincore A, Cook J, Tan F, El Halawany A, Riggins A, McDaniel S, Cook G, Martyshkin D V, Fedorov V V, Mirov S B, Shah L, Abouraddy A F, Richardson M C and Schepler K L 2018 *Opt. Express* **26** 7313